# Elucidating the Nuclear Quantum Dynamics of Intramolecular Double Hydrogen Transfer in Porphycene

Yair Litman,[†] Jeremy O. Richardson,[‡] Takashi Kumagai,[§] and Mariana Rossi*,[†]

[†]Theory Department, Fritz Haber Institute of the Max Planck Society, Faradayweg 4-6, 14195 Berlin, Germany
[‡]Laboratory of Physical Chemistry, ETH Zurich, 8093 Zurich, Switzerland
[§]Physical Chemistry Department, Fritz Haber Institute of the Max Planck Society, Faradayweg 4-6, 14195 Berlin, Germany

**S** Supporting Information

**ABSTRACT:** We address the double hydrogen transfer (DHT) dynamics of the porphycene molecule, a complex paradigmatic system in which the making and breaking of H-bonds in a highly anharmonic potential energy surface require a quantum mechanical treatment not only of the electrons but also of the nuclei. We combine density functional theory calculations, employing hybrid functionals and van der Waals corrections, with recently proposed and optimized path-integral ring-polymer methods for the approximation of quantum vibrational spectra and reaction rates. Our full-dimensional ring-polymer instanton simulations show that below 100 K the concerted DHT tunneling pathway dominates but between 100 and 300 K there is a competition between concerted and stepwise pathways when nuclear quantum effects are included. We obtain ground-state reaction rates of $2.19 \times 10^{11}$ s$^{-1}$ at 150 K and $0.63 \times 10^{11}$ s$^{-1}$ at 100 K, in good agreement with experiment. We also reproduce the puzzling N−H stretching band of porphycene with very good accuracy from thermostated ring-polymer molecular dynamics simulations. The position and line shape of this peak, centered at around 2600 cm$^{-1}$ and spanning 750 cm$^{-1}$, stem from a combination of very strong H-bonds, the coupling to low-frequency modes, and the access to *cis*-like isomeric conformations, which cannot be appropriately captured with classical-nuclei dynamics. These results verify the appropriateness of our general theoretical approach and provide a framework for a deeper physical understanding of hydrogen transfer dynamics in complex systems.
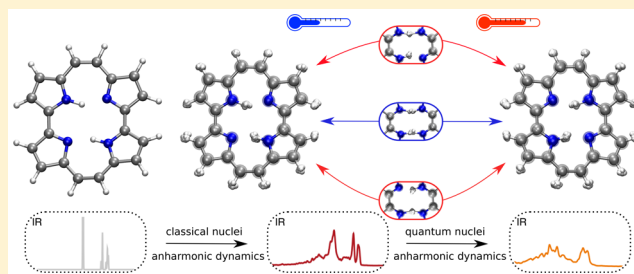
## INTRODUCTION

In hydrogen and proton transfer reactions,[1] electronic polarization and anharmonicities of the potential energy surface (PES) cause a considerable coupling between different degrees of freedom in the system, leading to complex intra- and intermolecular vibrational energy transfer.[2] In addition, because of the light mass of hydrogen, nuclear quantum effects (NQEs) such as tunneling and zero-point energy (ZPE) can play a crucial role at remarkably high temperatures,[3−7] and even heavy atoms (e.g., carbon or oxygen) can have an impact on hydrogen tunneling.[8,9] An accurate and quantitative description requires an all-atom, all-electron quantum simulation of these reactions and makes theoretical approaches based on empirical potentials and/or a dimensionality reduction of the PES, as well as a classical treatment of nuclear dynamics, inadequate.

Porphycene, the first synthesized structural isomer of free base porphyrin,[10] has emerged as a unique example of intramolecular double hydrogen transfer (DHT) in a multi-dimensional anharmonic PES, where strong hydrogen bonds are formed in the molecular cavity.[11,12] Interest in this molecule has increased in recent years, especially due to results obtained from scanning probe microscopy. Those have shown how different external stimuli, such as light,[13] heat,[14]

and force[15] can control the DHT, establishing this molecule as a prototype for the manufacture of rapid optical molecular switches and logic gates.

The presence of strong hydrogen bonds results in a low reaction barrier and a high DHT rate at room temperature ($k \approx 10^{12}$ s$^{-1}$)[16] compared to those of other derivatives, e.g., porphine ($k \approx 10^4$ s$^{-1}$).[17] The DHT reaction, which in this case connects the two degenerate *trans* tautomeric states (Figure 1), can occur through a stepwise or concerted mechanism. In the former case, the hydrogen atoms are transferred sequentially through an intermediate *cis* tautomeric state and the reaction pathway involves a first-order saddle point (SP1 in Figure 1). In the latter case, two hydrogen atoms are transferred in a correlated fashion without passing by a stable intermediate. This transfer can occur simultaneously through a second-order saddle point (SP2 in Figure 1), which is usually termed the synchronized mechanism.[18] It is also well established that the tautomerization reaction in the porphycene molecule is a multidimensional process. The strong vibrational level dependence of the tunneling splittings[19,20] and the modification of the tautomerization rate upon deuteration
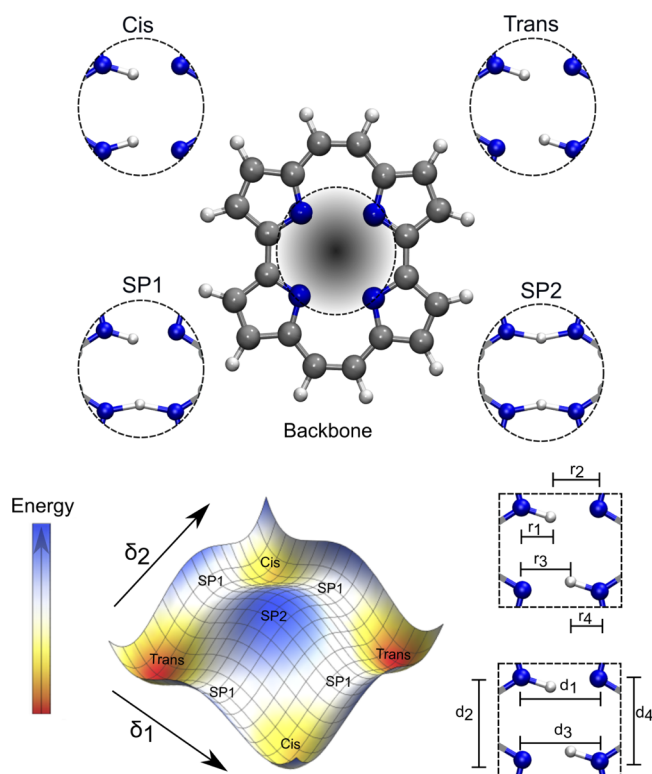
**Figure 1.** Characterization of the *cis* and *trans* isomers as well as a schematic two-dimensional (2D) potential energy surface (PES) of the porphycene molecule. SP1 and SP2 stand for first-order and second-order saddle points, respectively, and $r$ and $d$ are distances between atoms as marked in the figure. In the schematic 2D PES, $\delta_1 = r_1 - r_2$ and $\delta_2 = r_3 - r_4$.

of the peripheral hydrogens[21] are two manifestations of the multidimensional nature of the tunneling process. At cryogenic temperatures in the gas phase (or in a helium droplet), the vibrational ground-state level exhibits a tunneling splitting of 4.4 cm$^{-1}$,[19,20,22] showing that *trans–trans* tautomerization takes place via coherent tunneling through the concerted mechanism.[23,24] Indeed, excellent agreement with the experimental values has been obtained considering only this pathway.[25] However, vibrational couplings to the environment or, at higher temperatures, couplings to the intramolecular vibrational modes lead to decoherence of the wave function such that the quantum state decays exponentially and the reaction dynamics can be described as a rate process.[26] In these cases, which are more relevant for biological or technological applications, it is not straightforward to clarify which mechanism governs the DHT reaction, how temperature affects the reaction rates, and the character of the vibrational modes that play a role.

Vibrational spectroscopy is a powerful tool that can shed light on nuclear dynamics and the PES. The hydrogen stretching vibrational band in this system serves as a fingerprint of hydrogen bonding and can exhibit extremely complex spectral features, such as a broadening and the emergence of satellite peaks. In porphycene, the characterization of the N–H stretching mode ($\nu_{N-H}$) related to the *trans–trans* tautomerization has been particularly controversial, because of its apparent absence in the experimental Raman and infrared (IR) spectra, although theoretical calculations in the harmonic approximation predict a very intense band.[27] The broadening

of $\nu_{N-H}$ in porphycene resulting from the intermode coupling has been examined by a classical nuclear dynamics approach,[27] but an agreement between simulations and experiment could not be fully achieved. This suggests that a strongly anharmonic PES, intermode couplings, and NQEs all play a decisive role in the static and dynamic properties of the inner hydrogen atoms of porphycene.

The situation outlined above has long hampered the elucidation of the hydrogen bonding structure and tautomerization dynamics in porphycene. Approximations to the quantum dynamics have been reported, but they relied on a dimensionality reduction of the system and thus neglected vibrational coupling to several modes.[24,28−30] Classical molecular dynamics simulations that included the full dimensionality of the system but neglected the quantum nature of the nuclei have been performed.[27,31] Imaginary-time path-integral simulations based on a semiempirical PES have been carried out to compute quantum statistical properties but did not use a methodology that could access the real-time dynamics of the system (e.g., rates or vibrational spectra).[32,33] To date, an atomistic full-dimensional study of the quantum dynamics in this system has not been presented.

Here we demonstrate that all-atom and all-electron quantum simulations of porphycene can fully reveal the equilibrium and dynamical properties of this molecule in the gas phase and explain a variety of experimental observations. Employing newly implemented and optimized ring-polymer instanton theory[34] and the recently proposed ring-polymer molecular dynamics coupled to colored noise thermostats,[35] we assess in detail the open questions regarding the hydrogen bonding geometry, the hydrogen transfer dynamics, and the nature of the $\nu_{N-H}$ band observed in the IR spectrum using a first-principles PES without resorting to any dimensionality reduction. We show that the hydrogen transfer mechanism in porphycene follows non-intuitive pathways at certain temperatures, which underlines the significance of NQEs and intramolecular vibrational coupling.

## ■ RESULTS AND DISCUSSION

We first analyze the equilibrium properties of the porphycene molecule obtained from density functional theory (DFT-B3LYP+vdW) calculations and *ab initio* path-integral molecular dynamics (PIMD) simulations (see Methods). In Figure 2a, we show the free energy profile projected on the two hydrogen transfer coordinates $\delta_1$ and $\delta_2$ defined in Figure 1 for the PIMD simulation at 290 K. As expected, the *trans* isomer is the most energetically stable and the free energy barrier for hydrogen transfer is around 2 $k_BT$, in agreement with previous studies in which NQEs were also included.[32,33] For comparison, in the classical-nuclei *ab initio* molecular dynamics (MD) simulation at the same temperature, the hydrogen transfer reaction is a much rarer event with an effective barrier above 4 $k_BT$, as shown in the Supporting Information.

The stationary points of the free energy surface can be assigned to the *cis*, *trans*, first-order saddle point (SP1), and second-order saddle point (SP2) states of the molecule. While the exact boundary value ($b$) to distinguish different states is arbitrary due to the non-negligible density at all values connecting both states within the PIMD simulations, the *cis/trans* population ratio is robust for reasonable values of $0.1 < b < 0.3$, as shown in Figure S5. We calculate the *trans* population to be larger than the *cis* population by a factor 7. Note that these two-dimensional (2D) free energy surfaces are provided
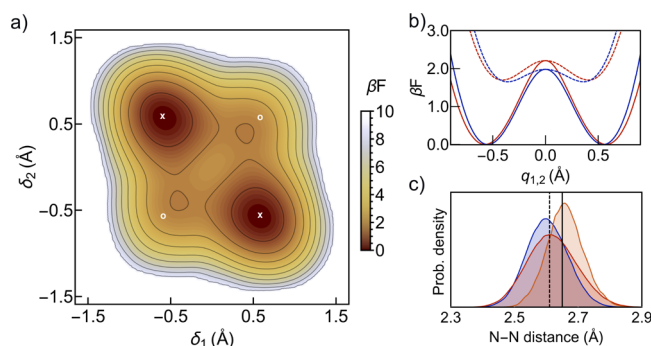
**Figure 2.** (a) Effective free energy profile of the porphycene molecule obtained from PIMD simulations at 290 K, projected on the $\delta_1$ and $\delta_2$ coordinates. The contour lines start at 0.75 $k_BT$ and are separated by 1 $k_BT$. The x and o symbols mark the position of the *trans* and *cis* conformers, respectively, when optimized at the potential energy surface. We define "*cis*-like" conformations as those lying in the vicinity of $(\delta_1, \delta_2)$ equal to $(+0.4, +0.4)$ or $(-0.4, -0.4)$. (b) Effective free energy projections along the $q_1$ ($\delta_1 = -\delta_2$) (solid lines) and $q_2$ ($\delta_1 = \delta_2$) (dashed lines) directions. Red and blue lines correspond to PIMD simulations at 290 and 100 K, respectively. (c) Nitrogen−nitrogen distance probability density obtained from PIMD simulations at 100 K (blue), PIMD simulations at 290 K (red), and MD simulation at 290 K (orange). Vertical lines indicate the minimum energy geometry values for the *trans* isomer (solid) and *cis* isomer (dashed).

as a guide to understand this system. All our calculations are carried out in the full $3N$-dimensional space.

The one-dimensional (1D) PIMD free energy projections along the $q_1$ and $q_2$ coordinates (defined along the lines $\delta_1 = -\delta_2$ and $\delta_1 = \delta_2$, respectively) are shown in Figure 2b at two temperatures, 290 and 100 K. These projections exhibit two interesting features. First, the effective energy difference between the wells, which within a first approximation would determine the *cis* and *trans* populations, does not change between 290 and 100 K. This means that in this temperature range only the lowest vibrational modes involving the N−H groups are populated and consequently the relative population is mostly governed by ZPE. The wells along $q_2$ (*cis*), however, are considerably softened toward the barrier when the temperature is reduced, while the wells along $q_1$ (*trans*) are not. This effectively increases the probability of *cis* conformations at lower temperatures. Second, decreasing the temperature has the surprising effect of decreasing the effective *trans*−*trans* free energy barrier by 10% and the *cis*−*cis* free energy barrier by 35%. This effect can be traced back to fluctuations in the cage dimensions. In Figure 2c, we show the probability density of the N−N distances, $d_1$ and $d_3$, defined in Figure 1. The quantum distribution at 290 K is broader and shifted to higher values in comparison to that at 100 K. The cage expansion at higher temperatures leads to an increase in the effective potential energy barrier for the hydrogen transfer reaction and is directly translated to the free energy profile. The smaller average N−N distances at lower temperatures correlate with an increased amount of *cis*-like conformations with respect to *trans* and are consistent with the strengthening of the hydrogen bonds observed from previous calculations on a reduced PES and NMR experiments.[29] In our PIMD simulations, we also observe that the average absolute value of the dipole projected along the H-bonded N atoms is 0.5 D, which is in contrast to the absent dipole moment of the *trans* minimum energy isomer. At the same time, it is also lower than

the corresponding dipole of the *cis* minimum energy isomer (1.2 D). This observation is consistent with the observed N−N distance distribution shown in Figure 2c, which is centered closer to the N−N distance of the optimal *cis* isomer when considering quantum nuclei. In the classical-nuclei simulations, the *cis*-like geometries are not visited at all and the cage is much larger.

At this point, it is worth noting that a reduction of the effective free energy barrier along the chosen reaction coordinate does not necessarily result in an increase in the hydrogen transfer rate. Within transition-state theory (TST), a probabilistic term that depends on the effective barrier height is multiplied by a dynamical correction factor (also called the transmission coefficient). It has been shown that the dynamical factor can have a temperature dependence that is much stronger than the probabilistic one.[36] Consequently, rates and barrier heights are not always trivially correlated and the temperature dependence of the rate obtained based exclusively on free energy barriers should be treated with caution. In fact, for this system, it is experimentally observed that the rates decrease with decreasing temperatures[26] and this is also what we find in our full-dimensional calculations shown below.

We now examine the quantum dynamical aspects of the hydrogen transfer reactions, which we approximate with ring-polymer instanton theory[37,38] and thermostated ring-polymer molecular dynamics.[39] We locate two instanton pathways, namely, the one related to the *trans*−*trans* concerted pathway and the one related to the *trans*−*cis* (−*trans*) stepwise pathway. Each instanton is a uniquely defined path that best describes a tunneling mechanism in porphycene. With these pathways, we can compute the thermal rate as $k = 2k_{step} + k_{conc}$[28] where $k_{step}$ and $k_{conc}$ are the rate constants corresponding to the concerted and stepwise mechanisms, respectively. The factor 2 takes into account the two possible *cis* intermediates. The ratios $R_s = 2k_{step}/k$ and $R_c = k_{conc}/k$ show the relative contribution of each pathway to the total observed double hydrogen transfer rate. The fact that we find two stable instanton pathways means that there are at least two independent pathways for the DHT. Even though we cannot guarantee that all possible DHT tunneling pathways are being considered, the symmetry of porphycene indicates that these should be the dominating (or the only) ones. Our best estimates for the DHT rates are listed in Table 1. These values are in good agreement with the

**Table 1. Calculated Hydrogen Transfer Rates ($k$) Compared to Experimental $k_{exp}$ Data from Reference 26, as Well as Tunneling Enhancement Factors ($\kappa_{tun}$), Contributions from the Concerted Path to the Rate $R_c = k_{conc}/k$, and Calculated Kinetic Isotope Effects (KIEs, $k^{HH}/k^{DD}$)**

|    | $T$ (K) | $k$ ($10^{11}$ s$^{-1}$) | $k_{exp}$ ($10^{11}$ s$^{-1}$) | $R_c$ | $\kappa_{tun}$ | KIE |
|----|---------|--------------------------|--------------------------------|-------|----------------|-----|
| HH | 150 | 2.190 | $1.62 \pm 0.04$ | 0.63 | 70 | |
| HH | 100 | 0.630 | $1.09 \pm 0.08$ | 0.95 | 1135 | |
| DD | 100 | 0.0025 | $0.03 \pm 0.02$ | 0.59 | 471 | 250 |

experimental values measured in solution. Direct comparison between our gas-phase calculation and these results in certain condensed-phase environments is supported by the observation of negligible solvent dependency in experiments.[40,41] In other types of environments such as surfaces[42,43] or polymer matrices,[44] the rate depends more strongly on the environment. Larger porphycene derivatives show rate dependency in both isotropic[41] and non-isotropic environments.[45]
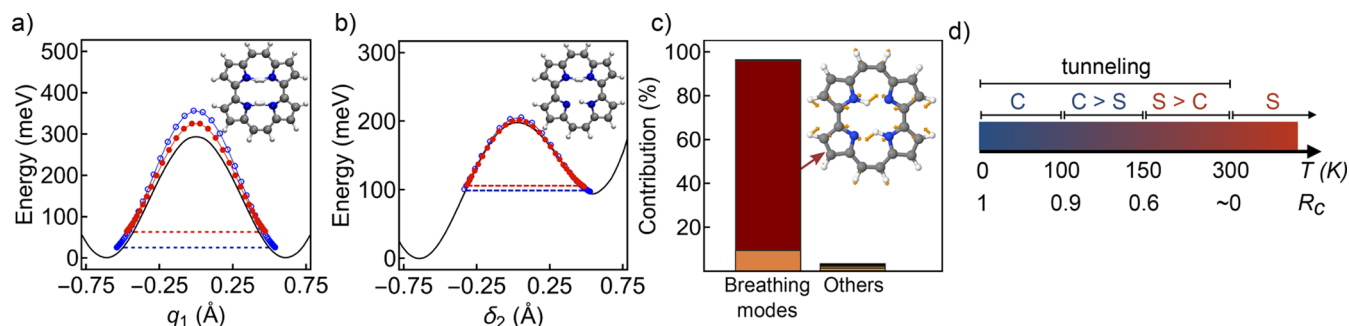
**Figure 3.** (a) Potential energies of different instanton imaginary-time slices along the *trans−trans* path at 100 K (empty blue circles) and 150 K (filled red circles). The black energy profile marks the ground-state potential energy surface, and the dashed lines mark the minimum energy of the intanton slices. (b) Same as in panel a for the *trans−cis* path. (c) Decomposition of the instanton turning point displacement of the *trans−trans* path into the mimimum energy *trans* geometry normal modes. The inset shows the breathing mode at 197 cm$^{-1}$ ($2A_g$) with the largest contribution. (d) Competition of different transfer mechanisms at different temperatures. C denotes the concerted mechanism, and S the stepwise mechanism. $R_c$ is the contribution from the concerted path to the rate as defined in the title of Table 1.

The tunneling enhancement factor, also reported in Table 1, is defined as $\kappa_{tun} = k_{inst}/k_{TST}$, where $k \equiv k_{inst}$ is the rate obtained with the instanton method and $k_{TST}$ is the rate obtained with the Eyring TST. As expected, tunneling effects thus increase the rates by almost 2 and 3 orders of magnitude at 150 and 100 K, respectively. More interestingly, at 150 K, the concerted and stepwise mechanisms make comparable contributions to the total rate, while at 100 K, the concerted path accounts for 95% of the rate. Note that if we neglect NQEs, the scenario is completely different: At both temperatures, the stepwise mechanism fully dominates.

This result can be understood in terms of the mechanisms predicted by the instanton pathways. In panels a and b of Figure 3, we show the minimum energy path (MEP) for the concerted *trans−trans* path and the stepwise *trans−cis* path, respectively, at 150 and 100 K (black solid curves). The barrier for the concerted path is higher than that of the stepwise one. Analyzing the tunneling paths themselves, we note that the stepwise path requires that the initial *trans* geometry be thermally excited to an energy comparable to that of the intermediate *cis* geometry, which is ~100 meV higher than the minimum, for tunneling to take place. From that point, the tunneling path follows quite closely the MEP and has essentially no temperature dependence between 100 and 150 K. In contrast, the concerted path enables tunneling at an energy close to the bottom of the well. The energy at which the system tunnels in this mechanism is temperature-dependent and is defined by instanton theory to give the optimal balance of the probability of barrier penetration and the probability of thermal excitation.[38] At 100 K, the tunneling path starts 25 meV above the minimum and reaches points above 350 meV. At 150 K, because more thermal energy is available, the path starts at 64 meV but does not reach such high values, keeping closer to the MEP.

At low temperatures, only the concerted mechanism is possible because there is not enough thermal energy available to reach the high-energy conformation at which the stepwise path takes place. The concerted mechanism presents a larger effective path length because two particles need to tunnel, and consequently, the microcanonical tunneling probability is always smaller than that for the stepwise case (see the Supporting Information). For this reason, increasing the available thermal energy strongly favors the stepwise mechanism. Indeed, above the crossover temperature of this system,[46] $T_c = \hbar\omega^*/2\pi k_B \approx 300$ K, where in most cases the

contribution to the rate from classical hopping over the barrier becomes more important than tunneling, the stepwise mechanism is dominant. Previous evidence of the stepwise mechanism at 300 K from classical-nuclei molecular dynamics simulations reported in ref 31 benefits from this fact, but those simulations would not be able to predict the intricate balance between the two mechanisms at lower temperatures. Our calculated DHT mechanisms at different temperatures are summarized schematically in Figure 3d.

The competition of both mechanisms below $T_c$ is compatible with some previous 2D model studies.[23] However, it goes against the common experimental interpretation that this reaction happens exclusively through the concerted path at any (low) temperature.[21,47] In particular, the lack of *cis* conformers observed in fluorescence anisotropy studies is treated as an indirect evidence for the concerted mechanism.[16,40] We propose that this is not a conclusive observation. The energy difference between the two isomers results in a very small *cis* population, and because of the low barrier height for the *cis−trans* reaction, any transient *cis* isomer will have a very short lifetime. Therefore, anisotropy measurements performed so far cannot rigorously confirm the mechanism in this particular scenario. Another possible experimental strategy for discerning the DHT mechanism is to monitor kinetic isotope effects (KIEs) upon substitution of two (DD) internal hydrogens by deuterium.[17] However, because of the lack of well-defined $\nu_{HH}$ and $\nu_{DD}$ bands, it has been difficult to interpret and quantify the isotopic purity of any sample. The KIE can be easily accessed via our calculations, and we report in Table 1 the DHT rate and the KIE for the DD isotopologue of porphycene at 100 K. KIEs from instanton theory benefit from error cancellations[48] that make them typically more reliable than direct rate calculations. Nonetheless, our calculated KIE is 7 times higher than what was reported from experiments.[26] This discrepancy would be consistent with an error in the theoretical barrier width with respect to experiment, especially for the stepwise mechanism. Indeed, we are correcting the B3LYP+vdW barrier height with data from CCSD(T) but cannot correct the barrier width with the available data. Because the *trans−trans* pathway is symmetric and the *trans−cis* (stepwise) pathway is not, correcting only the barrier should work better for the former. The deuterium rate at 100 K involves a large fraction of the stepwise mechanism contribution and thus is prone to a larger error. From our simulations, we find that the DHT mechanism itself

changes upon isotopic substitution, with deuteration strongly favoring the stepwise path as reflected by $R_c$. This situation is different for porphyrin, where there is no competition between the different pathways already for HH, such that it was possible to confirm the dominance of the stepwise mechanism from experiments.[17]

Our full-dimensional description allows us to go one step further and understand mode coupling in this DHT in more detail. We employ the normal mode decomposition proposed in ref 25 to analyze mode-specific contributions to tunneling splittings in porphycene. We take the *trans* isomer normal modes to decompose the displacement between the geometry from where the tunneling takes place (the instanton turning point) of the concerted path and the global minimum. Our decomposition, shown in Figure 3c, shows that >87% of the displacement is given by the breathing mode of the molecular cage at ~200 cm$^{-1}$ (24 meV). The coupling of the concerted DHT to this low-energy mode implies a temperature dependence for this reaction rate at low temperatures that can look like an Arrhenius behavior, despite the massive contribution from tunneling. Therefore, we show that the concerted mechanism is related to the temperature dependence of the rate at low temperatures measured in refs 26 and 47, which is consistent with a barrier of 22 meV and the previous suggestion that this vibrational mode contributes to the DHT. A novel insight that we gain from our simulations is that we can unambiguously explain the origin of the activation barrier for the second thermally activated channel reported in ref 26. From Figure 3b, it is apparent that for the stepwise tunneling path to be activated, the *cis* conformer minimum energy needs to be reached. Detailed balance thus imposes an effective activation energy for this mechanism equal to the *trans* to *cis* energy difference. Our best estimate for this value is 107 meV [CCSD(T) with MP2 ZPE corrections], which matches the experimentally inferred activation barrier of 108 ± 9 meV.

The signature of anharmonic intermode coupling and quantum contributions in the DHT is directly reflected in the vibrational fingerprints that appear in an IR spectrum. We compare in Figure 4 the IR spectra obtained with the quantum harmonic approximation (QH), the (anharmonic) time-correlation formalism with classical-nuclei dynamics (CL) at 290 K, and the same formalism with the approximation to quantum-nuclei dynamics from TRPMD (QA) at the same temperature (see Methods). We also present the experimental IR spectrum reported in ref 27. Below 1700 cm$^{-1}$ this spectrum was measured for porphycene in a CS$_2$ solution and above 1700 cm$^{-1}$ for porphycene in a KBr matrix.

Our calculated QH and CL spectra are in good agreement with the theoretical simulations previously presented in ref 27. As discussed there, (classical-nuclei) anharmonicities play an important role in $\nu_{N-H}$ at ~2900 cm$^{-1}$ (which can be easily assigned via normal mode analysis) and coupling to low-frequency vibrations considerably broadens the peak. However, the band is still present and shows a shape different from that of the experimentally measured spectrum at 290 K from ref 27. With the inclusion of NQEs, this peak is red-shifted by 300 cm$^{-1}$ and broadened, producing a very weak signal, remarkably similar to the experimental line shape. We observe a constant shift of only ≈40 cm$^{-1}$ between our simulations and experiment, which likely originates from the B3LYP+vdW PES. We corroborated the N−H stretch character of this peak by comparing spectra from hydrogenated and deuterated
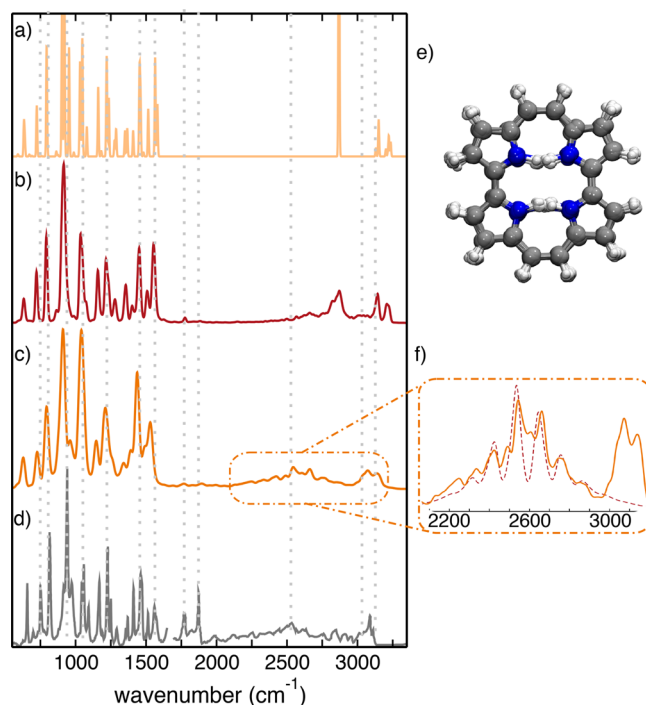


**Figure 4.** Porphycene IR spectra obtained through the (a) harmonic approximation, (b) Fourier transform of the dipole autocorrelation function from DFT-B3LYP+vdW trajectories with classical nuclei at 290 K, and (c) Fourier transform of the dipole autocorrelation function from DFT-B3LYP+vdW trajectories with quantum nuclei at 290 K from TRPMD. (d) Experimental spectra as reported in ref 27. Below 1700 cm$^{-1}$ this spectrum was measured for porphycene in a CS$_2$ solution and above 1700 cm$^{-1}$ for porphycene in a KBr matrix. The harmonic spectrum was artificially broadened with Gaussian functions for better visualization, and all of the theoretical spectra have a constant red-shift of 40 cm$^{-1}$. Dotted lines serve as guides to the eye. (e) Representative snapshots of the trajectory with quantum nuclei where all of the replicas are superimposed. (f) Close-up of the Fourier transform of the TRPMD IR spectrum in the N−H stretching mode region (orange) together with the adiabatic model (red dashed line) described in the text.

molecules (see Figure S9). The overtone peaks just below 2000 cm$^{-1}$ that were also observed in ref 27 are present in our CL and QA simulations, albeit with an intensity much lower than that of the experimental bands. This discrepancy in intensities could stem from the fact that both CL and QA spectra cannot capture quantum coherence. It could also stem from a particular enhancement of these bands due to the KBr matrix in experiment or to the laser power profile. To resolve this issue, comparison to gas-phase experimental spectra at lower temperatures would be desirable, but such data are not available. Overall, the results presented here show that NQEs are essential for quantitatively explaining the softening of the $\nu_{N-H}$ band and resolving its apparent absence from the experimental spectrum.[27,49]

One can relate this line shape also to the N−N distance distributions shown in Figure 2c. The shorter N−N distances in the path-integral simulations point to a strengthening of the H-bonds, which is related to the mode softening (red-shift). Characterizing the strength of mode couplings and the fine structure of this band, however, requires a deeper analysis, especially due to the fact that, as shown in Figure 4e, the hydrogens are delocalized over the several energy wells.

We follow the approach suggested in ref 50 that provides a way of calculating IR line shapes for coupled low- and high-frequency vibrational modes, which we detail in the Supporting Information. We used the adiabatic model, including direct damping (relaxation of the high-frequency mode) and indirect damping (relaxation of the low-frequency mode that is coupled to the high-frequency one). The most relevant parameters of the model are the high-frequency ($\Omega$) and low-frequency ($\omega$) values as well as the strength of the coupling between them ($\alpha$). As shown in Figure 4f, the agreement of the model with the TRPMD IR spectrum is good, especially for the fine structure of the mode. Because this model disregards hydrogen transfer and the DHT occurs on very long time scales compared to the N−H vibration, we safely conclude that DHT does not contribute to the line shape of this peak, similar to recent reports regarding the formic acid dimer.[51] The parameters for the curve shown in Figure 4f are reported in the Supporting Information. We can obtain good agreement for 2680 cm$^{-1}$ < $\omega$ < 2750 cm$^{-1}$ and 100 cm$^{-1}$ < $\Omega$ < 115 cm$^{-1}$, with corresponding $\alpha$ values ranging from 0.70 to 0.85. The exact value of $\Omega$ most likely reflects an effective value that averages the coupling to several low-frequency cage vibration modes. The coupling parameter $\alpha$ is more than 1 order of magnitude larger than a simple evaluation in the strong anharmonic coupling theory[52] based on harmonic modes, reflecting the enhancement of coupling due to anharmonic NQE. Notably, the $\omega$ values are very illuminating. They lie between the *trans* (2907 cm$^{-1}$) and *cis* (2680 cm$^{-1}$) harmonic frequency values. This shows the importance of visiting *cis*-like structures, which is only possible due to tunneling and ZPE contributions.

## CONCLUSIONS

In this paper, we have presented a combination of techniques joining high-level density functional theory simulations and state-of-the-art path-integral-based approximations to nuclear quantum dynamics that provides a deep physical understanding of hydrogen transfer reactions. We validated the predictive power of our approach through comparison with experimental data.

In particular, we have shown that in an accurate potential energy surface, NQEs involved in hydrogen transfer events can qualitatively change the dynamical properties of the porphycene molecule. Our calculated full-dimensional ring-polymer instanton rate of DHT is in good agreement with experiment at different temperatures. From our simulations, we are able to quantitatively obtain the relative contribution from the stepwise and the concerted DHT mechanisms at any temperature. We conclude that both tunneling pathways make a similar contribution to the rate at 150 K and that only below 100 K does the concerted pathway become dominant. We corroborate that the skeletal low-frequency vibration that couples to the DHT coordinate leads to an Arrhenius-like temperature dependence for the rate, even when the DHT is dominated by tunneling. Additionally, we show that the contribution of the stepwise pathway down to low temperatures explains the second thermally activated reaction channel reported in experiments.

From the path-integral simulations, we have shown how NQEs can strengthen N−H···N bonds, modify the N−N distances, and shift peaks up to 300 cm$^{-1}$. The coupling and delocalization of the hydrogens within the cage explain the apparent absence of the N−H stretch band in the IR spectrum of this molecule, which had long puzzled researchers. The IR spectrum calculated from thermostated ring-polymer molecular dynamics yields an exquisite agreement with the experimental line shape of $\nu_{N-H}$, even for the fine structure of the peak. We could reproduce this line shape with a simple model of coupled quantum harmonic oscillators, which allowed us to confirm that the coupling of this mode to low-frequency vibrations is enhanced when NQEs are included.

A shortcoming of increasing the complexity is that a detailed quantitative understanding of vibrational mode coupling can be compromised. Techniques like vibrational configuration interaction can, nevertheless, provide quantitative numbers even for rather complex molecules.[53] Techniques based on dynamics, however, do not give direct access to coupling coefficients without the application of other models.[54] The adiabatic model we employed in this work could give a qualitative explanation of the coupling and fine structure of the N−H stretching mode in the IR spectrum. Mode-specific experimental and theoretical techniques, like time-resolved 2D spectroscopy, would be necessary for a quantitative characterization of mode coupling at finite temperatures in high-dimensional systems. Nevertheless, the approaches presented here pave the way for addressing important problems in biology, related to enzymatic reactions through low-barrier H-bonds[55] and unusual fingerprints of N−H···N bonds in proteins,[56] and modeling functional materials that take advantage of hydrogen transfer events.[57−59]

## METHODS

We performed CCSD(T) calculations extrapolated to the infinite basis-set limit to obtain benchmarks for the energetics of local minima and saddle points of porphycene (see more details in the Supporting Information). We then compared less expensive exchange-correlation (xc) functionals within density functional theory (DFT) to these benchmarks and concluded that the B3LYP functional,[60] including pairwise van der Waals (vdW) corrections,[61] presented the best agreement with our reference for both energetic and geometrical properties. We thus chose this functional to perform all further electronic structure calculations in this work. The Orca package[62] was used to perform CCSD(T) simulations, and the FHI-aims[63] package for DFT simulations.

The nuclear degrees of freedom were sampled according to the B3LYP+vdW PES with MD and PIMD through the i-PI program[34,64] in connection with FHI-aims. The PIMD simulations were performed coupled to the colored noise PIGLET thermostat.[65] We were therefore able to use 6 and 12 beads for 290 and 100 K simulations, respectively.

Thermal rates were calculated with instanton rate theory.[37,38] The instanton path represents an approximation to the optimal tunneling pathway at a given temperature and can be determined for the full high-dimensional problem. We used the ring-polymer approach[66−69] in which the path is discretized and represented by $P$ beads in a harmonic ring polymer,[70] through our recent implementation in the i-PI code.[34] We include all 108 porphycene degrees of freedom in the path optimization. We have achieved convergence with 192 replicas at both 100 and 150 K (see the Supporting Information). This corresponds to a simulation involving, effectively, 7296 atoms with first-principles and on-the-fly force evaluations. We included a correction factor in the instanton action detailed in the Supporting Information, which linearly scales the action to match the CCSD(T) reference barrier, similar to that in ref 71.

Restarting an instanton calculation with a larger number of replicas can be computationally expensive due to the necessity of calculating all Hessians for the new amount of replicas. To overcome this bottleneck, we have derived and implemented in i-PI a ring-polymer expansion of the Hessian, given by $\mathcal{H}_{jm}^{(k)} = \sum_{s=1}^{P} H_{jm}^{(s)} T(P', P)_{ks}$,

where $P < P'$ and $H_{jm}^{(s)}$ is the $jm$ matrix element of the Hessian corresponding to the $s$th original replica and $\mathcal{H}_{jm}^{(k)}$ is the $jm$ matrix element of the Hessian corresponding to the $k$th expanded replica. The $P' \times P$ matrix $T(P', P)$ is the same transformation matrix used in other contraction/expansion approaches and given in ref 72. We provide the derivation of this expression in the Supporting Information. This procedure completely removes the necessity of calculating any new Hessians during the optimization, after their calculation for the first ring-polymer geometry with a small number of beads (replicas).

The IR spectra were computed from the Fourier transform of the dipole autocorrelation function. The classical-nuclei correlation function was computed from four different 10 ps *NVE* trajectories. An approximation to the quantum correlation function was computed using thermostated ring-polymer molecular dynamics[39] coupled to generalized Langevin equation (TRPMD+GLE) thermostats, as described in ref 35. In this case, we ran 7 different 10 ps trajectories using 16 beads (see convergence tests in the Supporting Information) and computed the dipole for all beads. In all cases, the starting configurations were taken from uncorrelated thermalized structures and we used a 0.5 fs time step for the integration of the equations of motion.

## ■ ASSOCIATED CONTENT

### Ⓢ Supporting Information

The Supporting Information is available free of charge on the ACS Publications website at DOI: 10.1021/jacs.8b12471.

Additional information regarding convergence tests, instanton rates, and simulations of vibrational spectra (PDF)

## ■ AUTHOR INFORMATION

### Corresponding Author
*rossi@fhi-berlin.mpg.de

### ORCID Ⓞ
Takashi Kumagai: 0000-0001-7029-062X
Mariana Rossi: 0000-0002-3552-0677

### Notes
The authors declare no competing financial interest.

## ■ ACKNOWLEDGMENTS

## ■ REFERENCES

(1) Hynes, J. T.; Klinman, J. P.; Limbach, H.; Schowen, R. L. *Hydrogen-Transfer Reactions*; Wiley-VCH Verlag GmbH and Co. KGaA, 2007.

(2) Warshel, A. Dynamics of reactions in polar solvents. Semi-classical trajectory studies of electron-transfer and proton-transfer reactions. *J. Phys. Chem.* **1982**, *86*, 2218−2224.

(3) Tuckerman, M. E.; Marx, D.; Klein, M. L.; Parrinello, M. On the Quantum Nature of the Shared Proton in Hydrogen Bonds. *Science* **1997**, *275*, 817−820.

(4) Marx, D.; Tuckerman, M. E.; Hutter, J.; Parrinello, M. The nature of the hydrated excess proton in water. *Nature* **1999**, *397*, 601−604.

(5) Klinman, J. P.; Kohen, A. Hydrogen Tunneling Links Protein Dynamics to Enzyme Catalysis. *Annu. Rev. Biochem.* **2013**, *82*, 471−496.

(6) Meisner, J.; Kästner, J. Atom Tunneling in Chemistry. *Angew. Chem., Int. Ed.* **2016**, *55*, 5400−5413.

(7) Rossi, M.; Ceriotti, M.; Manolopoulos, D. E. Nuclear Quantum Effects in H⁺ and OH⁻ Diffusion along Confined Water Wires. *J. Phys. Chem. Lett.* **2016**, *7*, 3001−3007.

(8) Tuckerman, M. E.; Marx, D. Heavy-Atom Skeleton Quantization and Proton Tunneling in "Intermediate-Barrier" Hydrogen Bonds. *Phys. Rev. Lett.* **2001**, *86*, 4946−4949.

(9) Hinsen, K.; Roux, B. Potential of mean force and reaction rates for proton transfer in acetylacetone. *J. Chem. Phys.* **1997**, *106*, 3567−3577.

(10) Vogel, E.; Köcher, M.; Schmickler, H.; Lex, J. Porphycene - a Novel Porphin Isomer. *Angew. Chem., Int. Ed. Engl.* **1986**, *25*, 257−259.

(11) Fita, P.; Grill, L.; Listkowski, A.; Piwonski, H.; Gawinkowski, S.; Pszona, M.; Sepiol, J.; Mengesha, E.; Kumagai, T.; Waluk, J. Spectroscopic and microscopic investigations of tautomerization in porphycenes: condensed phases, supersonic jets, and single molecule studies. *Phys. Chem. Chem. Phys.* **2017**, *19*, 4921−4937.

(12) Waluk, J. Spectroscopy and Tautomerization Studies of Porphycenes. *Chem. Rev.* **2017**, *117*, 2447−2480.

(13) Böckmann, H.; Liu, S.; Mielke, J.; Gawinkowski, S.; Waluk, J.; Grill, L.; Wolf, M.; Kumagai, T. Direct Observation of Photoinduced Tautomerization in Single Molecules at a Metal Surface. *Nano Lett.* **2016**, *16*, 1034−1041.

(14) Kumagai, T.; Hanke, F.; Gawinkowski, S.; Sharp, J.; Kotsis, K.; Waluk, J.; Persson, M.; Grill, L. Thermally and Vibrationally Induced Tautomerization of Single Porphycene Molecules on a Cu(110) Surface. *Phys. Rev. Lett.* **2013**, *111*, 246101.

(15) Ladenthin, J. N.; Frederiksen, T.; Persson, M.; Sharp, J. C.; Gawinkowski, S.; Waluk, J.; Kumagai, T. Force-induced tautomerization in a single molecule. *Nat. Chem.* **2016**, *8*, 935−940.

(16) Fita, P.; Urbańska, N.; Radzewicz, C.; Waluk, J. Ground- and Excited-State Tautomerization Rates in Porphycenes. *Chem. - Eur. J.* **2009**, *15*, 4851−4856.

(17) Braun, J.; Koecher, M.; Schlabach, M.; Wehrle, B.; Limbach, H.-H.; Vogel, E. NMR Study of the Tautomerism of Porphyrin Including the Kinetic HH/HD/DD Isotope Effects in the Liquid and the Solid State. *J. Am. Chem. Soc.* **1994**, *116*, 6593−6604.

(18) Dewar, M. J. S. Multibond reactions cannot normally be synchronous. *J. Am. Chem. Soc.* **1984**, *106*, 209−219.

(19) Mengesha, E. T.; Sepioł, J.; Borowicz, P.; Waluk, J. Vibrations of porphycene in the S0 and S1 electronic states: Single vibronic level dispersed fluorescence study in a supersonic jet. *J. Chem. Phys.* **2013**, *138*, 174201.

(20) Vdovin, A.; Waluk, J.; Dick, B.; Slenczka, A. Mode-Selective Promotion and Isotope Effects of Concerted Double-Hydrogen Tunneling in Porphycene Embedded in Superfluid Helium Nano-droplets. *ChemPhysChem* **2009**, *10*, 761−765.

(21) Mengesha, E. T.; Zehnacker-Rentien, A.; Sepioł, J.; Kijak, M.; Waluk, J. Spectroscopic Study of Jet-Cooled Deuterated Porphycenes: Unusual Isotopic Effects on Proton Tunneling. *J. Phys. Chem. B* **2015**, *119*, 2193−2203.

(22) Sepioł, J.; Stepanenko, Y.; Vdovin, A.; Mordziński, A.; Vogel, E.; Waluk, J. Proton tunnelling in porphycene seeded in a supersonic jet. *Chem. Phys. Lett.* **1998**, *296*, 549−556.

(23) Smedarchina, Z.; Siebrand, W.; Fernández-Ramos, A. Correlated double-proton transfer. I. Theory. *J. Chem. Phys.* **2007**, *127*, 174513.

(24) Smedarchina, Z.; Siebrand, W.; Fernández-Ramos, A. Tunneling splitting in double-proton transfer: Direct diagonalization results for porphycene. *J. Chem. Phys.* **2014**, *141*, 174312.

(25) Homayoon, Z.; Bowman, J. M.; Evangelista, F. A. Calculations of Mode-Specific Tunneling of Double-Hydrogen Transfer in Porphycene Agree with and Illuminate Experiment. *J. Phys. Chem. Lett.* **2014**, *5*, 2723−2727.

(26) Ciacka, P.; Fita, P.; Listkowski, A.; Radzewicz, C.; Waluk, J. Evidence for Dominant Role of Tunneling in Condensed Phases and at High Temperatures: Double Hydrogen Transfer in Porphycenes. *J. Phys. Chem. Lett.* **2016**, *7*, 283−288.

(27) Gawinkowski, S.; Walewski, L.; Vdovin, A.; Slenczka, A.; Rols, S.; Johnson, M. R.; Lesyng, B.; Waluk, J. Vibrations and hydrogen bonding in porphycene. *Phys. Chem. Chem. Phys.* **2012**, *14*, 5489−5503.

(28) Smedarchina, Z.; Shibl, M.; Kühn, O.; Fernandez-Ramos, A. The tautomerization dynamics of porphycene and its isotopomers: Concerted versus stepwise mechanisms. *Chem. Phys. Lett.* **2007**, *436*, 314−321.

(29) Shibl, M. F.; Pietrzak, M.; Limbach, H.-H.; Kühn, O. Geometric H/D Isotope Effects and Cooperativity of the Hydrogen Bonds in Porphycene. *ChemPhysChem* **2007**, *8*, 315−321.

(30) McKenzie, R. H. A diabatic state model for double proton transfer in hydrogen bonded complexes. *J. Chem. Phys.* **2014**, *141*, 104314.

(31) Walewski, L.; Waluk, J.; Lesyng, B. Car-Parrinello Molecular Dynamics Study of the Intramolecular Vibrational Mode-Sensitive Double Proton-Transfer Mechanisms in Porphycene. *J. Phys. Chem. A* **2010**, *114*, 2313−2318.

(32) Yoshikawa, T.; Sugawara, S.; Takayanagi, T.; Shiga, M.; Tachikawa, M. Quantum tautomerization in porphycene and its isotopomers: Path-integral molecular dynamics simulations. *Chem. Phys.* **2012**, *394*, 46−51.

(33) Yoshikawa, T.; Sugawara, S.; Takayanagi, T.; Shiga, M.; Tachikawa, M. Theoretical study on the mechanism of double proton transfer in porphycene by path-integral molecular dynamics simulations. *Chem. Phys. Lett.* **2010**, *496*, 14−19.

(34) Kapil, V.; Rossi, M.; Marsalek, O.; Petraglia, R.; Litman, Y.; Spura, T.; Cheng, B.; Cuzzocrea, A.; Meißner, R. H.; Wilkins, D. M.; Juda, P.; Bienvenue, S. P.; Fang, W.; Kessler, J.; Poltavsky, I.; Vandenbrande, S.; Wieme, J.; Corminboeuf, C.; Kühne, T. D.; Manolopoulos, D. E.; Markland, T. E.; Richardson, J. O.; Tkatchenko, A.; Tribello, G. A.; Van Speybroeck, V. V.; Ceriotti, M. i-PI 2.0: A universal force engine for advanced molecular simulations. *Comput. Phys. Commun.* **2019**, *236*, 214−223.

(35) Rossi, M.; Kapil, V.; Ceriotti, M. Fine tuning classical and quantum molecular dynamics using a generalized Langevin equation. *J. Chem. Phys.* **2018**, *148*, 102301.

(36) Craig, I. R.; Manolopoulos, D. E. A refined ring polymer molecular dynamics theory of chemical reaction rates. *J. Chem. Phys.* **2005**, *123*, 034102.

(37) Miller, W. H. Semiclassical limit of quantum mechanical transition state theory for nonseparable systems. *J. Chem. Phys.* **1975**, *62*, 1899−1906.

(38) Richardson, J. O. Perspective: Ring-polymer instanton theory. *J. Chem. Phys.* **2018**, *148*, 200901.

(39) Rossi, M.; Ceriotti, M.; Manolopoulos, D. E. How to remove the spurious resonances from ring polymer molecular dynamics. *J. Chem. Phys.* **2014**, *140*, 234116.

(40) Ciaćka, P.; Fita, P.; Listkowski, A.; Kijak, M.; Nonell, S.; Kuzuhara, D.; Yamada, H.; Radzewicz, C.; Waluk, J. Tautomerism in Porphycenes: Analysis of Rate-Affecting Factors. *J. Phys. Chem. B* **2015**, *119*, 2292−2301.

(41) Gil, M.; Dobkowski, J.; Wiosna-Sałyga, G.; Urbańska, N.; Fita, P.; Radzewicz, C.; Pietraszkiewicz, M.; Borowicz, P.; Marks, D.; Glasbeek, M.; Waluk, J. Unusual, solvent viscosity-controlled tautomerism and photophysics: Meso-alkylated porphycenes. *J. Am. Chem. Soc.* **2010**, *132*, 13472−13485.

(42) Koch, M.; Pagan, M.; Persson, M.; Gawinkowski, S.; Waluk, J.; Kumagai, T. Direct Observation of Double Hydrogen Transfer via Quantum Tunneling in a Single Porphycene Molecule on a Ag(110) Surface. *J. Am. Chem. Soc.* **2017**, *139*, 12681−12687.

(43) Kumagai, T.; Ladenthin, J. N.; Litman, Y.; Rossi, M.; Grill, L.; Gawinkowski, S.; Waluk, J.; Persson, M. Quantum tunneling in real space: Tautomerization of single porphycene molecules on the (111) surface of Cu, Ag, and Au. *J. Chem. Phys.* **2018**, *148*, 102330.

(44) Piatkowski, L.; Schanbacher, C.; Wackenhut, F.; Jamrozik, A.; Meixner, A. J.; Waluk, J. Nature of Large Temporal Fluctuations of Hydrogen Transfer Rates in Single Molecules. *J. Phys. Chem. Lett.* **2018**, *9*, 1211−1215.

(45) Piwoński, H.; Sokołowski, A.; Kijak, M.; Nonell, S.; Waluk, J. Arresting Tautomerization in a Single Molecule by the Surrounding Polymer: 2,7,12,17-Tetraphenyl Porphycene. *J. Phys. Chem. Lett.* **2013**, *4*, 3967−3971.

(46) Gillan, M. J. Quantum-classical crossover of the transition rate in the damped double well. *J. Phys. C: Solid State Phys.* **1987**, *20*, 3621−3641.

(47) Gil, M.; Waluk, J. Vibrational Gating of Double Hydrogen Tunneling in Porphycene. *J. Am. Chem. Soc.* **2007**, *129*, 1335−1341.

(48) Richardson, J. O.; Pérez, C.; Lobsiger, S.; Reid, A. A.; Temelso, B.; Shields, G. C.; Kisiel, Z.; Wales, D. J.; Pate, B. H.; Althorpe, S. C. Concerted Hydrogen-Bond Breaking by Quantum Tunneling in the Water Hexamer Prism. *Science* **2016**, *351*, 1310−1313.

(49) Malsch, K.; Hohlneicher, G. The Force Field of Porphycene: A Theoretical and Experimental Approach. *J. Phys. Chem. A* **1997**, *101*, 8409−8416.

(50) Henri-Rousseau, O.; Blaise, P. *Advances in Chemical Physics*; Wiley-Blackwell, 2008; Chapter 5, pp 245−496.

(51) Qu, C.; Bowman, J. M. High-dimensional fitting of sparse datasets of CCSD(T) electronic energies and MP2 dipole moments, illustrated for the formic acid dimer and its complex IR spectrum. *J. Chem. Phys.* **2018**, *148*, 241713.

(52) Henri-Rousseau, O.; Blaise, P. *Quantum Oscillators*; Wiley-Blackwell, 2011; Chapter 10, pp 279−313.

(53) Qu, C.; Bowman, J. M. Quantum and classical IR spectra of $(HCOOH)_2$, $(DCOOH)_2$ and $(DCOOD)_2$ using ab initio potential energy and dipole moment surfaces. *Faraday Discuss.* **2018**, *212*, 33.

(54) Mathias, G.; Baer, M. D. Generalized Normal Coordinates for the Vibrational Analysis of Molecular Dynamics Simulations. *J. Chem. Theory Comput.* **2011**, *7*, 2028−2039.

(55) Cleland, W. W.; Frey, P. A.; Gerlt, J. A. The Low Barrier Hydrogen Bond in Enzymatic Catalysis. *J. Biol. Chem.* **1998**, *273*, 25529−25532.

(56) Adhikary, R.; Zimmermann, J.; Liu, J.; Forrest, R. P.; Janicki, T. D.; Dawson, P. E.; Corcelli, S. A.; Romesberg, F. E. Evidence of an Unusual N−H⋯N Hydrogen Bond in Proteins. *J. Am. Chem. Soc.* **2014**, *136*, 13474−13477.

(57) Ueda, A.; Yamada, S.; Isono, T.; Kamo, H.; Nakao, A.; Kumai, R.; Nakao, H.; Murakami, Y.; Yamamoto, K.; Nishio, Y.; Mori, H. Hydrogen-Bond-Dynamics-Based Switching of Conductivity and Magnetism: A Phase Transition Caused by Deuterium and Electron Transfer in a Hydrogen-Bonded Purely Organic Conductor Crystal. *J. Am. Chem. Soc.* **2014**, *136*, 12184−12192.

(58) Sunairi, Y.; Ueda, A.; Yoshida, J.; Suzuki, K.; Mori, H. Anisotropic Proton Conductivity Arising from Hydrogen-Bond Patterns in Anhydrous Organic Single Crystals, Imidazolium Carboxylates. *J. Phys. Chem. C* **2018**, *122*, 11623−11632.

(59) Horiuchi, S.; Tokunaga, Y.; Giovannetti, G.; Picozzi, S.; Itoh, H.; Shimano, R.; Kumai, R.; Tokura, Y. Above-room-temperature ferroelectricity in a single-component molecular crystal. *Nature* **2010**, *463*, 789−792.

(60) Stephens, P. J.; Devlin, F. J.; Chabalowski, C. F.; Frisch, M. J. Ab Initio Calculation of Vibrational Absorption and Circular Dichroism Spectra Using Density Functional Force Fields. *J. Phys. Chem.* **1994**, *98*, 11623−11627.

(61) Tkatchenko, A.; Scheffler, M. Accurate Molecular Van Der Waals Interactions from Ground-State Electron Density and Free-Atom Reference Data. *Phys. Rev. Lett.* **2009**, *102*, 073005.

(62) Neese, F. The ORCA program system. *Wiley Interdiscip. Rev.: Comput. Mol. Sci.* **2012**, *110*, 73−78.

(63) Blum, V.; Gehrke, R.; Hanke, F.; Havu, P.; Havu, V.; Ren, X.; Reuter, K.; Scheffler, M. Ab initio molecular simulations with numeric atom-centered orbitals. *Comput. Phys. Commun.* **2009**, *180*, 2175−2196.

(64) Ceriotti, M.; More, J.; Manolopoulos, D. E. i-PI: A Python interface for ab initio path integral molecular dynamics simulations. *Comput. Phys. Commun.* **2014**, *185*, 1019−1026.

(65) Ceriotti, M.; Manolopoulos, D. E. Efficient First-Principles Calculation of the Quantum Kinetic Energy and Momentum Distribution of Nuclei. *Phys. Rev. Lett.* **2012**, *109*, 100604.

(66) Andersson, S.; Nyman, G.; Arnaldsson, A.; Manthe, U.; Jónsson, H. Comparison of Quantum Dynamics and Quantum Transition State Theory Estimates of the H + CH$_4$ Reaction Rate. *J. Phys. Chem. A* **2009**, *113*, 4468−4478.

(67) Richardson, J. O.; Althorpe, S. C. Ring-polymer molecular dynamics rate-theory in the deep-tunneling regime: Connection with semiclassical instanton theory. *J. Chem. Phys.* **2009**, *131*, 214106.

(68) Richardson, J. O. Ring-polymer instanton theory. *Int. Rev. Phys. Chem.* **2018**, *37*, 171−216.

(69) Rommel, J. B.; Goumans, T. P. M.; Kästner, J. Locating Instantons in Many Degrees of Freedom. *J. Chem. Theory Comput.* **2011**, *7*, 690−698.

(70) Chandler, D.; Wolynes, P. G. Exploiting the isomorphism between quantum theory and classical statistical mechanics of polyatomic fluids. *J. Chem. Phys.* **1981**, *74*, 4078−4095.

(71) Meisner, J.; Kästner, J. Dual-Level Approach to Instanton Theory. *J. Chem. Theory Comput.* **2018**, *14*, 1865−1872.

(72) Markland, T. E.; Manolopoulos, D. E. An efficient ring polymer contraction scheme for imaginary time path integral simulations. *J. Chem. Phys.* **2008**, *129*, 024105.